

# Effect of Extrusion Temperature on the Plastic Deformation of an Mg-Y-Zn Alloy Containing LPSO Phase Using *In Situ* Neutron Diffraction



G. GARCES, P. PEREZ, S. CABEZA, S. KABRA, W. GAN, and P. ADEVA

The evolution of the internal strains during *in situ* tension and compression tests has been measured in an MgY<sub>2</sub>Zn<sub>1</sub> alloy containing long-period stacking ordered (LPSO) phase using neutron diffraction. The alloy was extruded at two different temperatures to study the influence of the microstructure and texture of the magnesium and the LPSO phases on the deformation mechanisms. The alloy extruded at 623 K (350 °C) exhibits a strong fiber texture with the basal plane parallel to the extrusion direction due to the presence of areas of coarse non-recrystallised grains. However, at 723 K (450 °C), the magnesium phase is fully recrystallised with grains randomly oriented. On the other hand, at the two extrusion temperatures, the LPSO phase orients their basal plane parallel to the extrusion direction. Yield stress is always slightly higher in compression than in tension. Independently on the stress sign and the extrusion temperature, the beginning of plasticity is controlled by the activation of the basal slip system in the dynamic recrystallized grains. Therefore, the elongated fiber-shaped LPSO phase which behaves as the reinforcement in a metal matrix composite is responsible for this tension–compression asymmetry.

DOI: 10.1007/s11661-017-4284-6

© The Minerals, Metals & Materials Society and ASM International 2017

## I. INTRODUCTION

EXTRUDED Mg-Y-Zn alloys containing long-period stacking ordered (LPSO) phases combine at low density with high mechanical strength at room temperature and good creep resistance at intermediate temperatures.<sup>[1–6]</sup> The LPSO phase is a long-range stacking of basal planes with periodic enrichment of zinc and yttrium with a chemical order.<sup>[7,8]</sup> The microstructure of extruded LPSO-containing alloys and, therefore, their mechanical properties can be tailored by varying extrusion parameters, *i.e.*, extrusion temperature, extrusion rate, and extrusion ratio.<sup>[9]</sup> High mechanical strength (near 350 MPa) with appreciable ductility can be achieved decreasing the extrusion temperature up to 623 K (350 °C).<sup>[2]</sup> At this extrusion temperature, the alloy exhibits a microstructure consisting of a mixture of finely equiaxed and randomly oriented recrystallised  $\alpha$ -Mg grains (DRXed grains), coarse-elongated non-DRXed  $\alpha$ -Mg grains highly oriented with the basal plane parallel to the extrusion direction, and fiber-shaped LPSO phase elongated along

the extrusion direction also oriented with the basal plane parallel to the extrusion direction.

The contribution of each phase to the global mechanical behavior of the alloy is complex and depends on their volume fractions and the deformation mode, tension, or compression. DRXed fine magnesium grains contribute to ductility improvement because their random orientation favors the activation of the basal slip system. Moreover, they increase the mechanical strength of the alloy as the grain size is refined.<sup>[10,11]</sup> Yamasaki *et al.*<sup>[2]</sup> proposed that non-DRXed  $\alpha$ -Mg grains contribute to the mechanical strength of the alloy in tension since their orientation inhibited the activation of basal slip system. However, it has been reported that under compression they can easily deform plastically due to the activation of the tensile  $\{10\bar{1}\bar{1}\}\{10\bar{1}2\}$  twinning system.<sup>[12]</sup> The LPSO phase behaves as a reinforcement in metal matrix composites and reinforces the magnesium matrix due to their higher Young modulus.<sup>[10,13–15]</sup> Moreover, the strong texture built up during the extrusion process inhibits the activation of basal slip system during tensile or compressive testing. Under compression along the extrusion axis, the LPSO phase can deform by the activation of a kinking process.<sup>[16,17]</sup> It has been reported that the extruded LPSO phase exhibits a higher yield stress in compression than in tension<sup>[17]</sup> this asymmetry being opposite to that observed in magnesium and magnesium alloys.<sup>[18]</sup> Therefore, the “multicomponent” microstructure of LPSO-containing alloys will exhibit complex mechanical behavior. These alloys show a tension–compression asymmetry whose magnitude and sign depend on the volume fraction of LPSO phase as well as of deformed

G. GARCES, P. PEREZ, and P. ADEVA are with the Department of Physical Metallurgy, CENIM-CSIC, Avenida Gregorio del Amo 8, 28040 Madrid, Spain. Contact e-mail: ggarces@cenim.csic.es S. CABEZA is with the Department of Non-Destructive Testing, Federal Institute for Materials Research and Testing BAM, Berlin, Germany. S. KABRA is with the STFC, Rutherford Appleton Laboratory, ISIS Neutron Facility, Harwell OX11 0QX, UK. W. GAN is with the German Engineering Materials Center at MLZ, Helmholtz-Zentrum Geesthacht, 85747 Garching, Germany.

Manuscript submitted February 22, 2017.

Article published online August 14, 2017

and DRX grains.<sup>[19]</sup> Alloys with low volume fraction of LPSO phase (< 10 vol pct), with a high volume fraction of non-DRXed grains, show the typical behavior of extruded magnesium alloys where yield stress in tension is higher than in compression. This effect is, however, reversed as the volume fraction of the LPSO phase increases.<sup>[19]</sup> Randomly oriented DRXed grains control the beginning of plasticity due to the activation of the basal slip system. Therefore, they have the same plastic behavior under tension or compression and, then, the tension–compression asymmetry of Mg–Y–Zn alloys should be only controlled by the yield stress of the LPSO phase which is higher in a uniaxial compression test. This behavior should be independent on the crystal texture of the magnesium phase provided that the beginning of the plasticity is controlled by randomly oriented DRXed grains. This paper examines in detail this assumption using neutron diffraction during *in situ* tension and compression experiments. The Mg<sub>97</sub>Y<sub>2</sub>Zn<sub>1</sub> (at. pct) alloys with almost 20 vol pct volume fraction of LPSO phase are extruded at two temperatures, 623 K and 723 K (350 °C and 450 °C), to obtain two different microstructures and crystallographic textures in the magnesium matrix.

## II. EXPERIMENTAL PROCEDURE

The material studied has a composition of Mg<sub>97</sub>Y<sub>2</sub>Zn<sub>1</sub> (at. pct) and was prepared by melting in an electric furnace using high purity Mg and Zn elements and Mg–Y master alloy. Ingots were cast into a steel mold of diameter 42 mm and then extruded to 10 mm diameter bar (extrusion ratio 18:1) at 623 K and 723 K (350 °C and 450 °C). The extrusion pressure is reduced from around 1800 to 900 MPa due to the increase in the extrusion temperature.

Microstructural characterization of the alloys was carried out by scanning electron microscopy (SEM). Samples were prepared by mechanical polishing and finishing with an etching solution of 5 ml acetic acid, 20 ml water, and 25 ml picric acid in methanol. Quantitative image analysis was carried out to calculate the average grain size of the magnesium matrix after extrusion using the software Sigma Scan Pro. Furthermore, Orientation Image Maps were done by Electron Backscattered Diffraction (EBSD) technique coupled to a JEOL JSM 6500F. High-angle boundaries > 10 deg and low-angle boundaries > 2 deg are represented by black and white lines, respectively. Samples for EBSD experiments required a very carefully metallographical preparation because of the high reactivity of Mg. Thus the specimens were ground with 320, 600, 1200, and 2000 grit SiC paper, polished with a solution of colloidal silica in ethanol, and finally chemically etched with a cooled solution of 10 ml HNO<sub>3</sub>, 30 ml acetic acid, 40 ml H<sub>2</sub>O, and 120 ml ethanol.

The macroscopic texture of the magnesium phase was measured using neutron diffraction in the as-extruded state as well as after tension and compression deformation. Five complete pole figures were measured at STRESS-SPEC beamline located at FRM II (Garching,

Germany) with a wavelength of 1.74 Å from Ge (311) monochromator using the robot system.<sup>[20]</sup> The reference system was always selected with the Z axis parallel to the extrusion direction. The microscopic texture was also evaluated in the magnesium phase using EBSD. In this case, the reference system was selected with the X axis parallel to the extrusion direction. The texture of the LPSO phase was measured using synchrotron radiation diffraction at the P07—HEMS beamline of PETRA III, at the Deutsches Elektronen-Synchrotron (DESY). The main advantage of using synchrotron radiation instead of X-ray is to avoid the peak overlapping of magnesium and LPSO crystal structures that occurs for diffraction angles of “laboratory” X-rays. HEMS beamline allows reaching low diffraction angles avoiding this problem. The diffraction patterns consisting in Debye–Scherrer rings were recorded using an exposure time of 1 second by a PerkinElmer XRD 1622 flat-panel detector with an array of 2048<sup>2</sup> pixel, with an effective pixel size of 200×200 μm<sup>2</sup>. The beam energy was 100 keV, corresponding to a wavelength of 0.0124 nm. LaB<sub>6</sub> powders were used as a reference to calibrate the acquired diffraction spectra. The detector-to-sample distance was set to 1650 mm. Table I resumes the samples and set-up parameters in diffraction experiments.

The mechanical properties of the Mg<sub>97</sub>Y<sub>2</sub>Zn<sub>1</sub> alloy extruded at both temperatures, 623 K and 723 K (350 °C and 450 °C), were evaluated by conventional tension and compression tests as well as by *in situ* tension and compression tests in the beamline ENGIN-X along the extrusion direction.

In the first case, tests were carried out using an Instron universal testing machine at a constant strain rate of 10<sup>−4</sup> s<sup>−1</sup>. Cylindrical samples of diameter 3 mm and gage length 10 were used for tensile tests and cylinders of diameter 5 mm and high 10 mm for compression tests.

The *in situ* tensile and compressive tests were carried out in the beamline ENGIN-X at the ISIS spallation source.<sup>[21]</sup> ENGIN-X beamline is equipped with a universal Instron loading frame with its loading axis oriented at 45 deg to the incident neutron beam. Two detector banks placed at ±90 deg to the incident beam register the time-of-flight (TOF) neutron diffraction patterns in the axial and radial direction with respect to the loading direction simultaneously. The TOF diffraction patterns were collected upon step-wise loading in the elastic regime and in step-wise straining in the plastic regime. It is important to point out that a plastic relaxation takes place during the acquisition time in the plastic regime. Each reflection of the diffraction pattern is inherently associated with a subset of similarly oriented grains and reflects the average behavior of the particular subset of grains within the gage volume.

The cylindrical test specimens for tension (diameter = 5 mm, *l*<sub>0</sub> = 40 mm) and compression (diameter = 10 mm, *l*<sub>0</sub> = 20 mm) were machined from the as-extruded bar in the extrusion direction. The strain during tensile and compressive tests was measured using an extensometer located in the tensile or compressive samples.

The collected diffraction patterns were analyzed by a single-peak fitting routine using a pseudo-Voigt function

**Table I. Overview of Samples and Set-Up Parameters in Diffraction Experiments**

Geometry and Dimensions of Samples	Technique and Characterization	Source and Parameters
Cylinders Diameter: 5 mm Length = 10 mm	texture Mg (Z axis parallel to the extrusion direction) neutron diffraction:	STRESS-SPEC beamline (FRM II) 1.74 Å Ge-311 monochromator pixel size 1.42 detector-to-sample 840 mm, gage volume: coming beam size 15 mm, second slit open chi: 6 tilts (7.5-22.5-37.5-52.5-67.5-82.5 deg) phi: 0 to 360 deg continuous rotation, 2D imaged obtained at each 20 s (phi's ~2.5 deg) output grid 5 deg × 5 deg
Cylinders Diameter : 5 mm Length: 10 mm	synchrotron diffraction texture LPSO (axial direction parallel to the extrusion axis)	P07—HEMS beamline (PETRA III-DESY) PerkinElmer XRD 1622 flat-panel detector 2048 <sup>2</sup> pixel <sup>2</sup> effective pixel size of 200×200 μm <sup>2</sup> 100 keV (λ = 0.0124 nm) detector-to-sample 1650 mm gage volume: 5 × 1 × 1 mm <sup>3</sup> Acq. time 1 s
(a) Tensile Cylinder Diameter: 5 mm. Length: 40 mm.	neutron diffraction (TOF): <i>in situ</i> compression/tension evolution of internal strains of Mg and LPSO phase	ENGIN-X beamline (ISIS) dimension slits: tensile : 4 × 7 mm <sup>2</sup> compressive: 10 × 7 mm <sup>2</sup>
(a) Compressive Cylinder Diameter : 10 mm Length: 40 mm		

convoluted with two back-to-back exponentials. The elastic strain for each orientation can be calculated by the shift on the position of each diffraction peak

$$\varepsilon_{hkl} = \frac{d_{hkl} - d_{0,hkl}}{d_{0,hkl}}, \quad [1]$$

where  $d_{0,hkl}$  is the lattice spacing of the stress-free value.

### III. RESULTS

Figures 1(a) and (b) show the backscattered electron images of the as-extruded Mg<sub>97</sub>Y<sub>2</sub>Zn<sub>1</sub> alloy consisting of a magnesium matrix (darker) and the LPSO phase (brighter) elongated along the extrusion direction. The volume fraction of LPSO has been calculated previously with a value of 19 pct.<sup>[11]</sup> The Orientation Image Mapping (OIM) of Figures 1(c) and (d) indicates that during the extrusion process, a dynamic recrystallization (DRX) process of the magnesium matrix takes place. The grain structure in the alloy extruded at 623 K (350 °C) showed zones of fine grains fully recrystallised with a grain size of 0.9 μm and zones of coarse and elongated grains with a volume fraction of 57 and 24 pct, respectively.<sup>[11]</sup> On the other hand, the magnesium phase is fully recrystallised in the alloy extruded at 723 K (450 °C) with a grain size of 15 μm.

Figures 2(a), (b), (d), and (e) show the {10 $\bar{1}$ 0} and {0002} pole figures for the Mg<sub>97</sub>Y<sub>2</sub>Zn<sub>1</sub> alloy extruded at the two extruded temperatures. The alloy extruded at 623 K (350 °C) shows an intense fiber texture with

the basal plane parallel to the extrusion direction. This texture decreases for the extrusion temperature of 723 K (450 °C) showing a more random texture. Figures 2(c) and (f) show the (0002) pole figures obtained from EBSD images of Figures 1(c) and (d). The (0002) pole figure in the alloy extruded at 623 K (350 °C) shows that while the non-DRXed grains are highly oriented with the basal plane oriented parallel to the extrusion direction (see black circle in Figure 2(c)), the DRXed grains are randomly oriented. On the other hand, the (0002) pole figure in the alloy extruded at 723 K (450 °C) shows that grains of Figure 1(d) are randomly oriented in agreement with macro-texture.

Figure 3 shows the Debye–Scherrer rings obtained for the Mg<sub>97</sub>Y<sub>2</sub>Zn<sub>1</sub> alloy extruded at 323 K and 723 K (350 °C and 450 °C). The intensity of magnesium rings for the alloy extruded at 723 K (450 °C) is more homogenous as a function of the azimuthal angle due to its weaker texture. The inner ring which corresponds to the (0003) reflection of the 18R structure<sup>[22,23]</sup> reveals that the LPSO phase in both extrusion temperatures is oriented parallel to the extrusion direction, *i.e.*, the maximum is observed for 90 and 270 deg (see white arrows). However, in the case of the alloy extruded at 623 K (350 °C) LPSO phase is more highly oriented than in the alloy extruded at 723 K (450 °C) where intensity is spread toward axial direction.

Figure 4 shows the tension and compression curves for the Mg<sub>97</sub>Y<sub>2</sub>Zn<sub>1</sub> alloy extruded at 623 K and 723 K (350 °C and 450 °C). The mechanical strength of the alloy extruded at 623 K (350 °C) is higher (almost the double) compared to the alloy extruded at lower

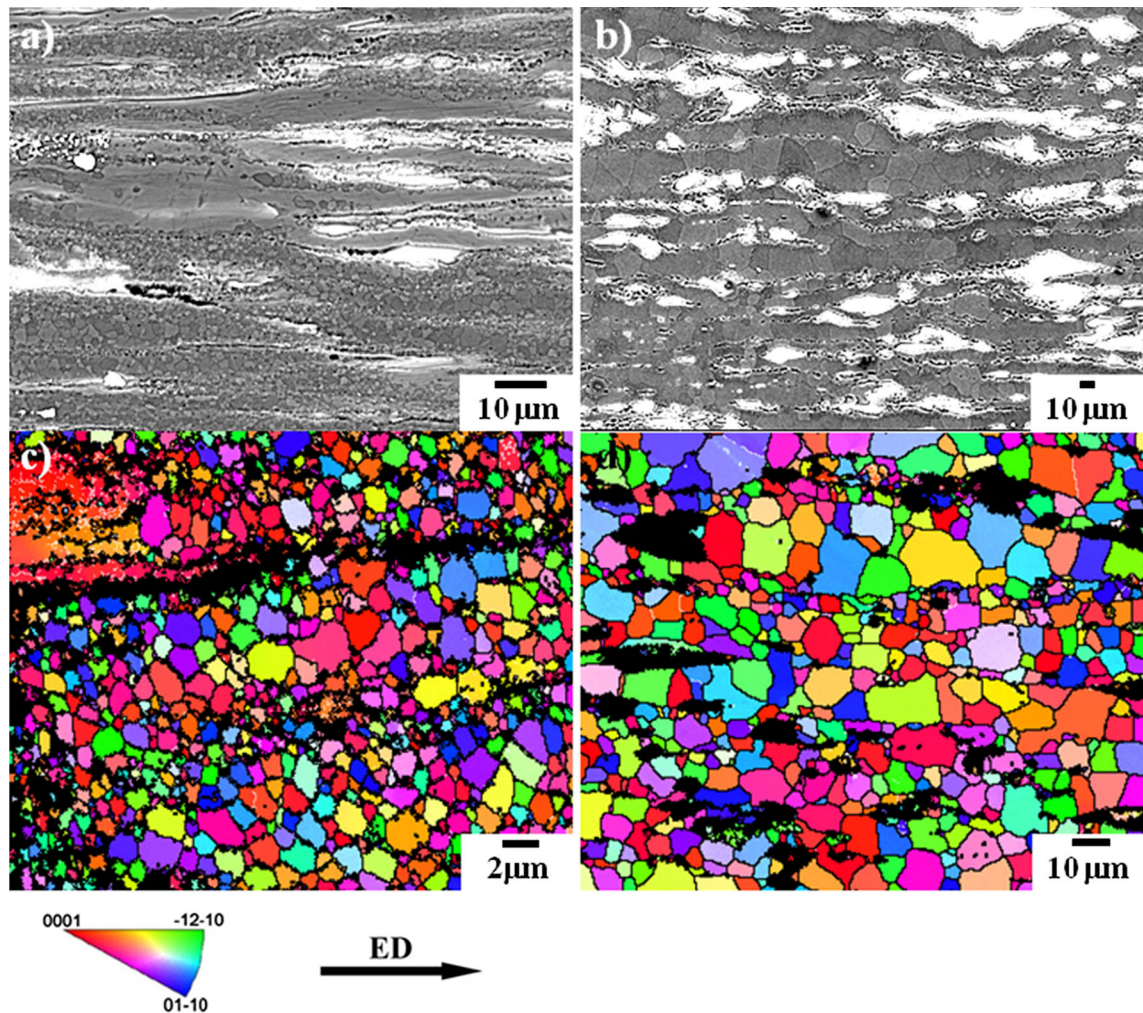


Fig. 1—Microstructure of the  $\text{MgY}_2\text{Zn}_1$  alloy extruded at (a) 623 K (350 °C) and (b) 723 K (450 °C). Color key triangle, EBSD results showing orientation image mapping (OIM) in the plane of ED-TD of the  $\text{MgY}_2\text{Zn}_1$  alloy extruded at (c) 623 K (350 °C) and (d) 723 K (450 °C).

temperature for tension and compression. Ductility, however, follows the opposite behavior.

The shape of the tension and compression curves is quite different, especially for the alloy extruded at the lowest temperature. While in tension, the curve shows the typical elasto-plastic behavior with a moderate work hardening after the elastic regime, the compression curve shows three zones of stress-strain behavior (see curve of  $\text{Mg}_{97}\text{Y}_2\text{Zn}_1$  alloy extruded at 62 K (350 °C)). At the beginning, the alloy shows an elastic regime up to a yield stress of around 376 MPa, after which the alloy flows exhibiting a steady stress plateau up to strain of around 3 pct. Finally, the stress increases rapidly up to the sample fracture stress. This shape of the stress-strain curve is explained because of the plastic deformation is controlled by twinning.<sup>[24]</sup> The stress plateau after yielding disappears in the alloy extruded at 723 K (450 °C). At both extrusion temperatures, yield stress in compression is higher than in tension and these differ-

ences are similar for both extrusion temperatures, around 20 to 30 MPa.

In order to study the deformation mechanism in  $\text{MgY}_2\text{Zn}_1$  alloy, the evolution of internal strains has been evaluated during *in situ* tension and compression tests for both extrusion temperatures. Figures 5(a) and (b) show the axial and radial diffraction patterns before tension or compression tests of the  $\text{MgY}_2\text{Zn}_1$  alloy extruded at 623 K and 723 K (350 °C and 450 °C), respectively. Diffraction peaks can be distinguished corresponding to the  $\{10\bar{1}0\}$ ,  $\{0002\}$ ,  $\{10\bar{1}1\}$ ,  $\{10\bar{1}2\}$ , and  $\{11\bar{2}0\}$  from magnesium phase and  $\{4228\}$  and  $\{42210\}$  from the LPSO phase. Although the intensity of diffraction peaks corresponding to the LPSO phase is small compared to those obtained from the magnesium phase, it is important to point out that these peaks can be fitted reliably.

The axial diffraction pattern is obtained from the planes close to perpendicular to the tension/compression axis (extrusion direction) and the radial diffraction

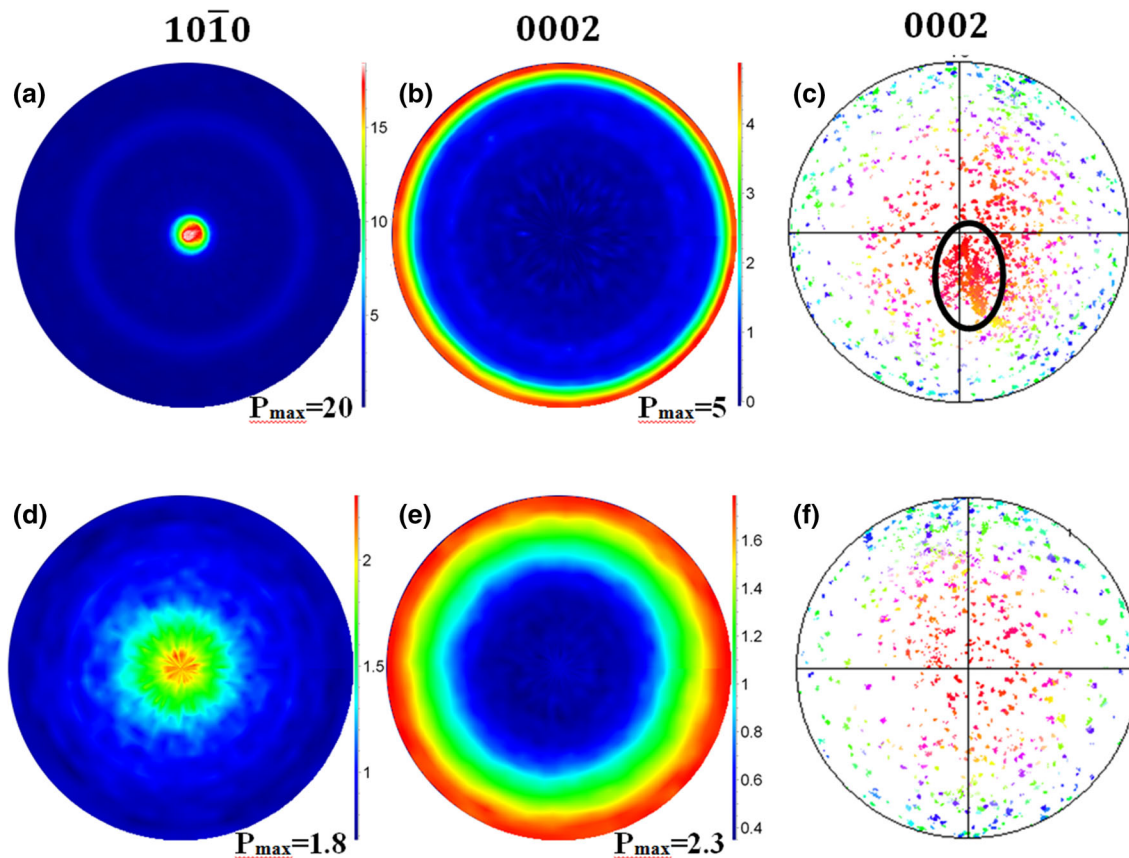


Fig. 2— $\{10\bar{1}0\}$  and  $\{0002\}$  pole figures obtained using neutron diffraction and  $\{0002\}$  pole figure obtained from EBSD of the of the  $\text{MgY}_2\text{Zn}_1$  alloy. (a) through (c) extruded 623 K (350 °C) and (d) through (f) extruded at 723 K (450 °C). (a) and (b) are obtained from Ref. [19]. The extrusion direction is normal to the measured surface of the sample for neutron diffraction and parallel to the  $X$  axis for EBSD.

pattern is obtained from planes parallel to the tension/compression axis. It is for this reason, and the strong fiber texture with the basal plane parallel to the extrusion direction in the alloy extruded at 623 K (350 °C), that the axial pattern shows a strong diffraction peak of the  $\{10\bar{1}0\}$  planes in contrast to the radial pattern, where the  $\{0002\}$  diffraction peak is the most intense peak. In the alloy extruded at 723 K (450 °C), where the magnesium phase is fully recrystallised and the texture was almost random (Figure 2), the axial and the radial patterns show that the strongest diffraction peak corresponds to  $\{10\bar{1}1\}$ .

Figure 6(a) through (d) shows the evolution of the elastic strain (obtained from the change of interplanar spacings as indicated in Eq. [1]) as a function of the applied stress in the axial and radial direction for  $\{10\bar{1}0\}$ ,  $\{0002\}$ ,  $\{10\bar{1}1\}$ , and  $\{11\bar{2}0\}$  diffraction peaks in the case of the magnesium phase and for  $\{42\bar{2}8\}$  and  $\{4\bar{2}2\bar{1}0\}$  diffraction peaks in the case of the LPSO phase during the tension and compression tests for the  $\text{MgY}_2\text{Zn}_1$  extruded at 623 K and 723 K (350 °C and 450 °C). The tensile and compressive curves obtained during *in situ* experiments are also plotted at the same scale indicating the macroscopic yield stress of the alloy. The analysis will concentrate on the axial stress–strain measurements, for which the strains are larger than

those measured from the radial diffraction data, although to a large extent the two are simply invertedly related in a Poisson-like relationship.

#### A. Alloys Extruded at 623 K (350 °C) with Bimodal Grain Structure

In the elastic regime in both tension and compression tests (Figure 6), the evolution of internal strains as a function of the applied stress of all diffracted peaks in the magnesium phase is linear and its slope, which represents the Young's Modulus, has similar values between 47 and 49 GPa. Magnesium alloys are known to be elastically isotropic and no differences of elastic strains between different orientations have been observed in the elastic regime<sup>[25]</sup> with a Young's modulus of 45 GPa.<sup>[26]</sup> Internal elastic strains in the LPSO phase also evolve linearly but with different linear slopes depending on each diffraction peak. Tane *et al.*<sup>[15]</sup> have demonstrated using resonant ultrasound spectroscopy that 18R structure is elastically anisotropic and the Young's modulus of the LPSO phase along  $c$  direction was clearly higher than that along a direction.

Since the alloy is formed by two highly plastic anisotropic phases, the evolution of internal strains in the plastic regime is difficult to explain together for both

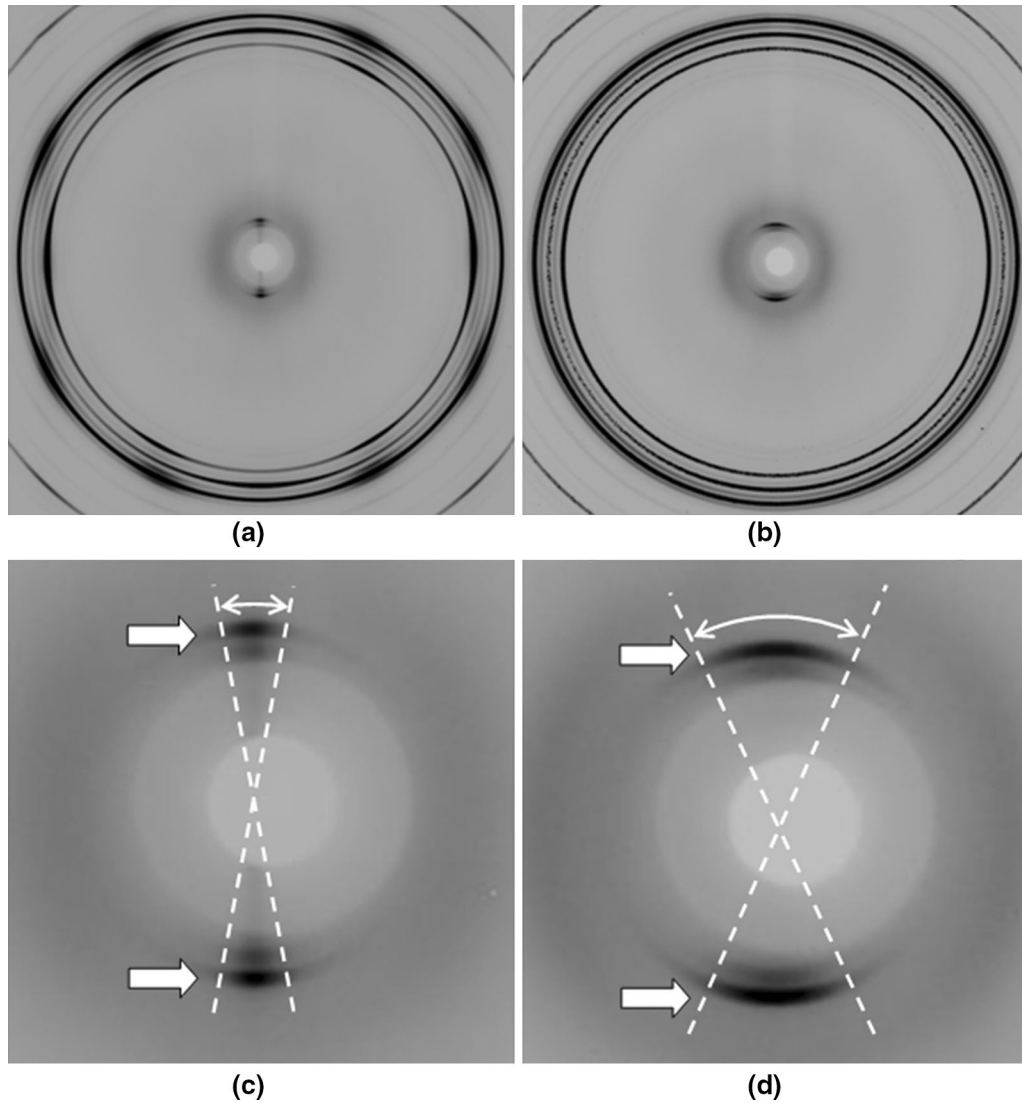


Fig. 3—Synchrotron diffraction pattern recorded on the 2D flat-panel detector after diffraction by the  $Mg_{97}Y_2Zn_1$  alloy extruded at (a) 623 K (350 °C) and (b) 723 K (450 °C) before compression. Diffraction ring corresponding to the (0003) plane of the 18R phase: (c) 623 K (350 °C) and (d) 723 K (450 °C).

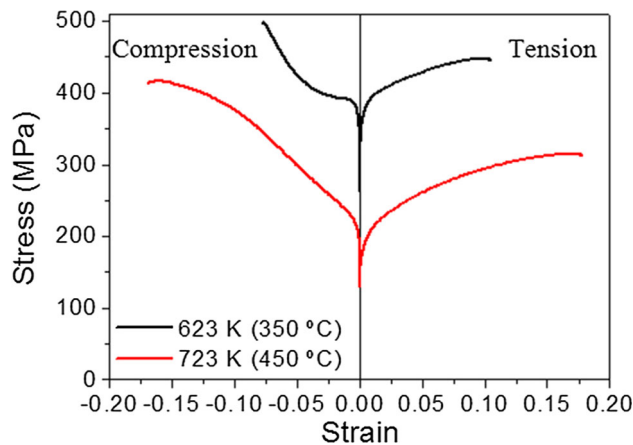


Fig. 4—Tensile (right side) and compressive (left side) curves for the  $Mg_{97}Y_2Zn_1$  alloy extruded at 623 K and 723 K (350 °C and 450 °C).

phases at the same time. Therefore, its evolution will be detailed separately, starting from the LPSO phase. As it was commented before, it was possible to fit it reliably throughout all tensile and compressive tests, although diffraction peaks of the LPSO phase were weak. However, it is important to mention that errors associated to elastic strains in the LPSO-diffracted peaks are one order of magnitude higher than those obtained in the magnesium phase.

In the tensile test, the LPSO phase seems to behave elastically to the macroscopic tensile yield stress, 325 MPa. At this point, elastic strains continued with the same slope than in the elastic regime (see {42210} diffraction peak) or increased to high tensile values (see {4228} diffraction peaks). This behavior suggests that after macroscopic yielding of the alloy, the LPSO phase supports a higher stress than the average applied stress confirming its reinforcing role.<sup>[13]</sup>

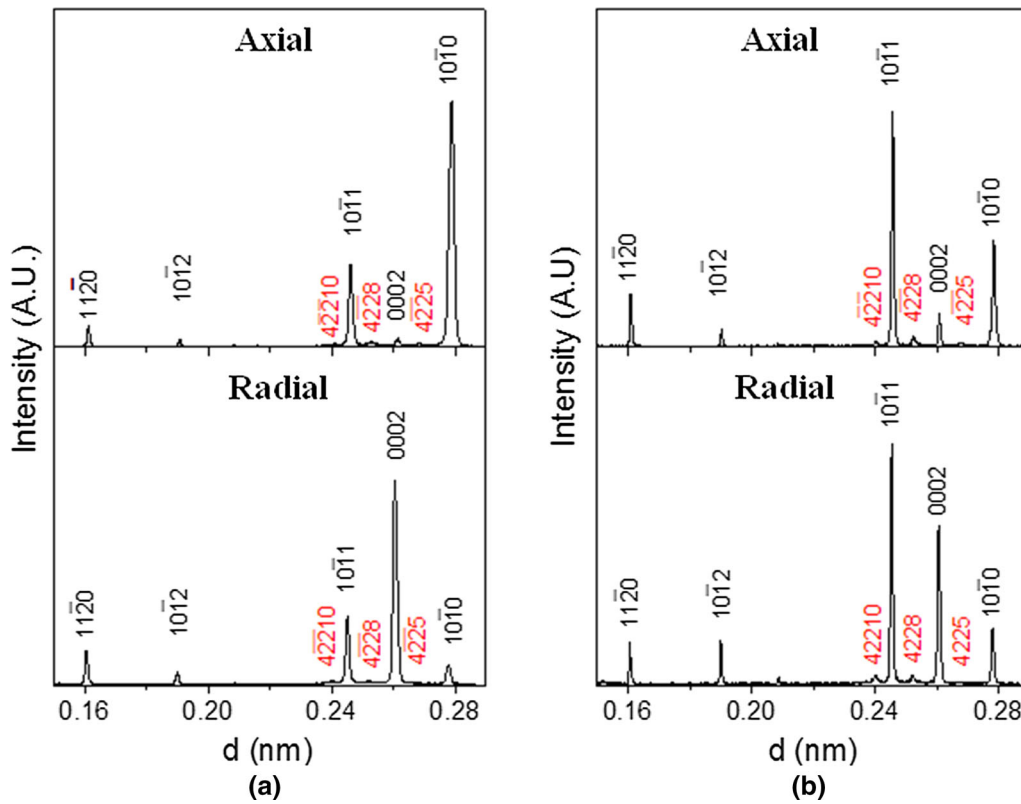


Fig. 5—Axial and radial diffraction patterns as a function of  $d$  of the extruded  $MgY_2Zn_1$  alloy extruded at (a) 623 K (350 °C) and (b) 723 K (450 °C).

In the compression test, the LPSO phase also behaves elastically to the macroscopic compressive yield stress, 350 MPa. At this stress, just as in case of the tensile test, elastic strains increased to high compressive values. However, this increase disappears at 400 MPa, where the elastic strains for the two LPSO diffraction peaks are constant. This fact would imply that LPSO phase is plastically deformed. It is expected that LPSO phase oriented with the basal plane parallel to the extrusion direction is deformed by kinking process.<sup>[16,17]</sup>

Figures 7(a) and (b) show the evolution of the elastic strain (equal of Figure 6) as a function of the applied stress in the axial direction only for  $\{10\bar{1}0\}$ ,  $\{0002\}$ ,  $\{10\bar{1}1\}$  and  $\{11\bar{2}0\}$  diffraction peaks of the magnesium phase for tensile and compressive tests. During tensile test, in the elastic regime shown in Figure 7(a), at stresses below about 325 MPa, the evolution of internal strains of all the diffracted peaks in the magnesium phase is linear with applied stress. Above 325 MPa,  $\{10\bar{1}1\}$ -oriented planes (grains) parallel to the stress/extrusion direction lose their elastic linearity. This stress corresponds closely to the yield stress (at 0.2 pct plastic strain). These grains are well oriented for deformation on the basal slip system,<sup>[25]</sup> and it is likely that macroscopic yielding occurs by the operation of this system. It is expected that elastic strains were constant when deformation is mainly controlled by plasticity. However, elastic strains corresponding to  $\{10\bar{1}1\}$  diffracted peaks decreased to lower tensile values from +6000  $\mu$ strains at 325 MPa to

+3000  $\mu$ strains at 425 MPa. Grains oriented with the  $\{0002\}$  planes perpendicular to the tensile direction (extrusion direction) continued showing elastic behavior above macroscopic yield up to around 375 MPa. At this point, elastic strains decreased to lower tensile values from +7000  $\mu$ strains to +5500  $\mu$ strains. Different to all the other planes, grains oriented with the  $\{10\bar{1}0\}$  and  $\{11\bar{2}0\}$  planes perpendicular to the tensile tests and related with the coarse-deformed grains show only elastic behavior in the full stress range up to the sample fracture. Grains with these orientations cannot plastically deform by the activation of the basal slip since Schmid factor is 0 under a stress along the extrusion direction. Moreover, the tensile stress along the extrusion direction induces a contraction of the  $c$ -axis in these grains avoiding the activation of tensile twinning.

Compared to the tensile behavior, the evolution of the elastic strains of the  $\{10\bar{1}0\}$ ,  $\{0002\}$ ,  $\{10\bar{1}1\}$ ,  $\{10\bar{1}2\}$ , and  $\{11\bar{2}0\}$  in compression is more complex. Before the stress plateau is reached, at a stress near 400 MPa (Figure 6(b)), lower than the macroscopic yield stress, the different magnesium diffraction peaks lose elastic linearity at different applied stresses, see Figure 7(b).

First, grains with (0002) planes perpendicular to the compression test (extrusion direction) exhibit a microyielding at an applied stress near 300 MPa which is considerably smaller than macroscopic yield stress at room temperature (350 MPa). The Schmid factor for the activation of basal slip in grains with this orientation is

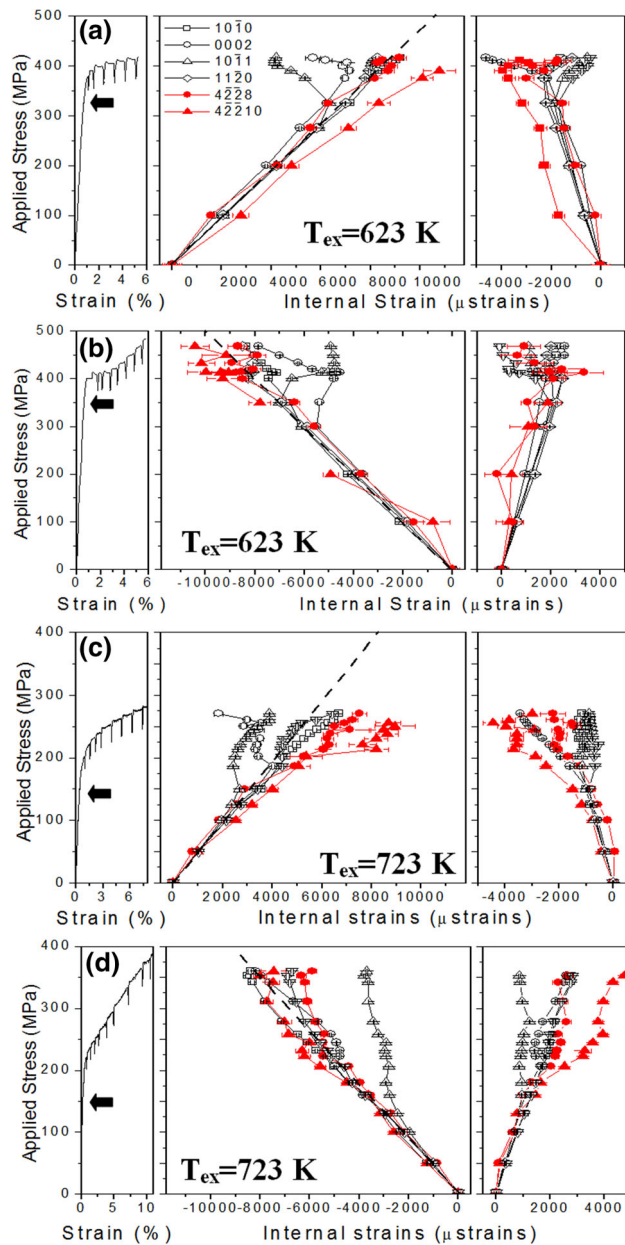


Fig. 6—Axial and radial internal strains as a function of the applied stress during *in situ* (a) and (c) tension and (b) and (d) compression tests at room temperature of the  $Mg_{97}Y_2Zn_1$  alloy. Macroscopic stress–strain curve is also plotted in the same scale. Open and solid symbols correspond to the magnesium and LPSO phases, respectively.

zero (with the stress applied along c directions) and tension  $\langle 10\bar{1}1 \rangle \{10\bar{1}2\}$  twinning cannot also be activated since compression generates a contraction of the c-axis in these grains. Recently, Garces *et al.*<sup>[12]</sup> have demonstrated that the microyielding observed in grains oriented with the basal plane perpendicular to the compression tests is an “artifact” caused due to the activation of tensile twinning in the coarse-deformed grains oriented with the basal plane parallel to the extrusion direction. Before twinning, (0002) planes in coarse-deformed grains are under elastic tension. Dur-

ing twinning, the (0002) planes within twins rotate 86 deg with respect to their initial orientation and are located perpendicular to the compression direction contributing to the (0002) diffraction peak in the axial direction.<sup>[25,27,28]</sup> These twins are surrounded by an elasto-plastic matrix which required a certain time to relax the tensile stress before going to compression stress. Therefore, the (0002) diffracted peak have two contributions: (i) the diffracted peak coming from DRXed grains that are moving towards higher compression strain and (ii) the diffracted peak of twins in the coarse-deformed grains that are under tension. Until a compressive stress state prevails in twins generated during compression, which takes place at 400 MPa, the internal strains of (0002) planes in the axial direction decrease their values. At this moment, the internal strains of the (0002) planes increase rapidly because twins can deform neither by dislocation slip in the basal system nor by twinning in the  $\langle 10\bar{1}1 \rangle \{10\bar{1}2\}$  tension system.

Figures 8(a) and (b) show the evolution of the integrated intensity in logarithmic scale for  $\{10\bar{1}0\}$ ,  $\{0002\}$ ,  $\{10\bar{1}1\}$ ,  $\{10\bar{1}2\}$ , and  $\{11\bar{2}0\}$  diffracted peaks of the magnesium phase and the  $\{4228\}$  diffracted peaks of LPSO phase during *in situ* tensile and compressive tests. While in the tension test intensity of all diffracted peaks are constant, in compression the intensity of the (0002) peak increases slightly in the microyield region (from about 300 to 400 MPa) and then increases rapidly above 400 MPa, corresponding to the stress plateau in the compression curve. At the same time, in contrast, the intensity of the  $\{10\bar{1}0\}$  peaks decreases steadily. This is in agreement with the  $\{10\bar{1}0\}$  and  $\{0002\}$  pole figures measured after the tensile and compressive test using neutron diffraction (Figure 9). In tension, there is no significant change compared with those obtained in the as-extruded material (Figure 9(a)). However, after uniaxial compression the crystal lattice rotate since the maximum of the  $\{10\bar{1}0\}$  and  $\{0002\}$  pole figures are observed near  $\theta = 90$  and 0 deg, respectively (Figure 9 (c)).

At 350 MPa (below the stress plateau), the  $\{10\bar{1}1\}$ -oriented grains parallel to the stress/extrusion direction lose their elastic linearity. This stress corresponds closely to the macroscopic yield stress in compression (at 0.2 pct plastic strain). These grains are well oriented for deformation on the basal slip system,<sup>[25]</sup> and therefore macroscopic yielding occurs by the operation of this system in DRXed grains.<sup>[12]</sup> As compression takes the overall stress level into the plateau regime, the internal strains of the  $\{10\bar{1}0\}$ -oriented planes (grains) parallel to the stress/extrusion direction evolve strongly decreasing from  $-7000 \mu\text{strains}$  at 325 MPa to  $-4500 \mu\text{strains}$  at 425 MPa. At this stress (400 MPa), the integrated intensities of the  $\{10\bar{1}0\}$  and (0002) diffraction peaks change significantly and it appears that extensive twinning continues. The internal strains of (0002) and  $\{10\bar{1}0\}$  planes increase rapidly, especially for the (0002) plane which shows a (macroscopic) stress–strain (internal) slope much lower than during the elastic regime. Above 425 MPa, internal strains of  $\{10\bar{1}1\}$ -oriented grains remain constant.



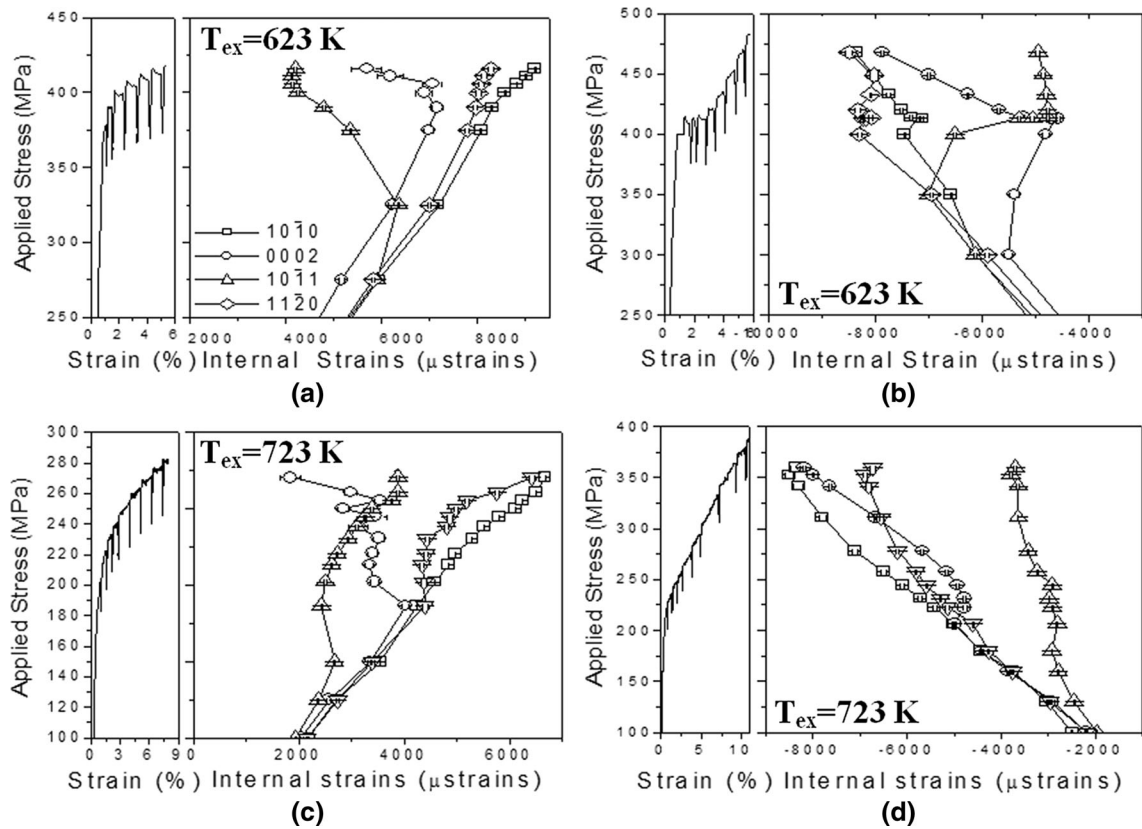


Fig. 7—Axial internal strains as a function of the applied stress during *in situ* (a) and (c) tension and (b) and (d) compression tests at room temperature of the  $Mg_{97}Y_2Zn_1$  alloy for the magnesium diffraction peaks. Macroscopic stress–strain curve is also plotted in the same scale.

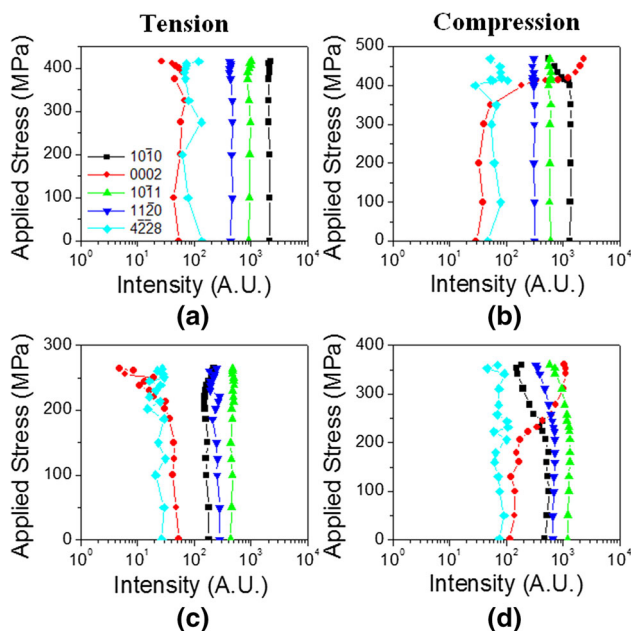


Fig. 8—Evolution of the integrated intensity of the  $\{10\bar{1}0\}$ ,  $\{0002\}$ ,  $\{10\bar{1}1\}$ , and  $\{11\bar{2}0\}$  diffraction peaks corresponding to magnesium phase and the  $\{42\bar{2}8\}$  diffraction peak of the LPSO phase during tension and compression tests of the  $MgY_2Zn_1$  alloy extruded at (a) and (c) 623 K (350 °C) and (b) and (d) 723 K (450 °C).

Finally, the  $\{11\bar{2}0\}$  planes and non-twinned areas of  $\{10\bar{1}0\}$  planes show only elastic behavior up to stress levels above this yield stress since basal slip is more difficult.

### B. Alloys Extruded at 723 K (450 °C) with a Fully Recrystallised Grain Structure

The evolution of internal strains in the alloy extruded at 723 K (450 °C) in the elastic regime as a function of the applied stress of all diffracted peaks in the magnesium phase is also linear and its slope is similar in both tension and compression tests (Figures 6(c) and (d)). The Young's modulus calculated from the slope between the stress and internal strains in the elastic regime has values between 44 and 46 GPa.

As in the case of the alloy extruded at 623 K (350 °C), the evolution of internal strain for the LPSO phase will be described first. In the tensile test, the LPSO phase seems to behave elastically to 150 MPa. Above this stress, the slope of the elastic strains as a function of the applied stress decreases. This means that the stress required to reach a certain elastic strains is less than that in the elastic zone. Therefore, since the yield stress in tension of the extruded LPSO is reported to be around 400 MPa,<sup>[17]</sup> the LPSO phase is assuming an additional

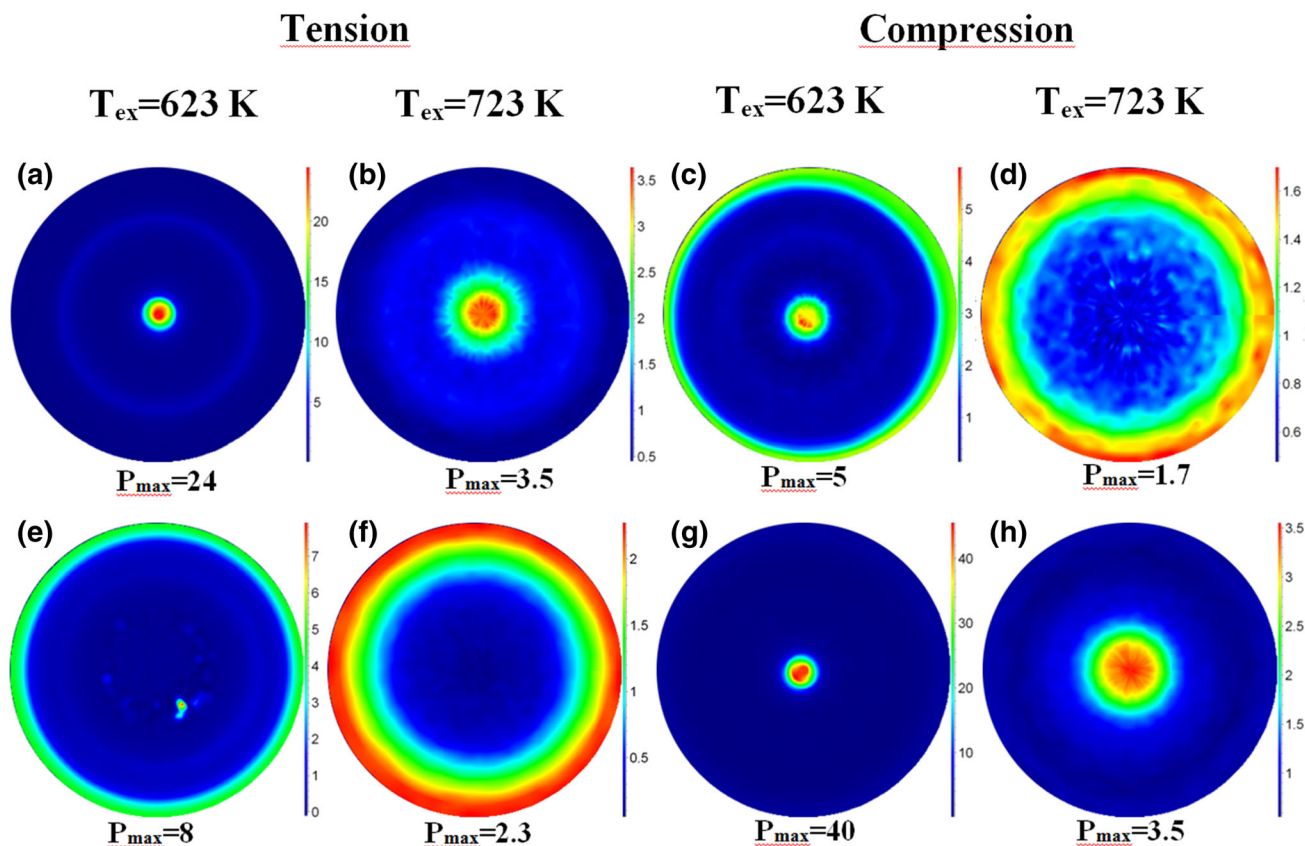


Fig. 9—Pole figure of (a) through (d)  $\{10\bar{1}0\}$  and (e) through (h)  $\{0002\}$  peaks in the extrusion condition and after tension and compression tests. (a), (c), (e), and (g) are obtained from Ref. [19].

load transferred by the magnesium matrix. In the compression test, the elastic strains in the LPSO phase also follow a similar behavior than in tension up to 250 MPa. At this stress, the elastic strains remain constant which it can be related with its yielding, probably by a kinking process.

Figures 7(c) and (d) show, separately, the evolution of the elastic strain as a function of the applied stress only in the axial direction the diffraction peaks of the magnesium phase for tensile and compressive tests. For the alloy extruded at 723 K (450 °C), this behavior is much more similar for tension and compression. Equal to the alloy extruded at 623 K (350 °C), in the elastic regime shown in Figure 7(a), at stresses below about 150 MPa, the evolution of internal strains of all the diffracted peaks in the magnesium phase is linear with applied stress. Above 150 MPa,  $\{10\bar{1}1\}$ -oriented planes (grains) parallel to the stress/extrusion direction lose their elastic linearity. This stress corresponds closely to the yield stress (at 0.2 pct plastic strain). These grains are well oriented for plastic deformation on the basal slip system, and it is probably that macroscopic yielding occurs by the operation of this system which has the lower critically resolved shear stress.

Grains oriented with the  $\{0002\}$  planes perpendicular to the tensile direction (extrusion direction) continued showing elastic behavior above macroscopic yield up to around 200 MPa. At this point, in the tension test, elastic strains decreased to lower tensile values from +4000  $\mu$ strains to +3000  $\mu$ strains and remains constant. The Schmid factor for the activation of basal slip in these grains is zero. Therefore, the loss of linearity should be related with other types of slip or twinning systems. At this stress, the intensity of the  $\{0002\}$  diffraction peak (Figure 8(c)) decreases accompanied by the increase in the intensity of the  $\{10\bar{1}0\}$  diffraction peak. This exchange of intensity between  $\{10\bar{1}0\}$  and  $\{0002\}$  diffraction peaks is connected with the tensile twinning. These grains are well oriented for the activation of the twinning system since tension along the extrusion direction induces an elongation of the c-axis in these grains.

On the other hand, in compression at around 200 MPa, the elastic strains corresponding to the  $\{0002\}$  diffraction peak also lose their linearity and they are constant up to around 250 MPa. Then, they decrease continuously with a linear slope as in the alloy extruded at 623 K (350 °C). The intensity of the  $\{0002\}$  diffraction peak increases while the

intensity of the  $\{10\bar{1}0\}$  diffraction peak decreases (Figure 8(d)), similar to the behavior of the alloy extruded at 623 K (350 °C) (Figure 8(b)). However, the intensity of the  $\{0002\}$  diffraction peak after compression is higher than the alloy extruded at 623 K (350 °C) due to its higher texture in the as-extruded condition.

Different to all the other planes, grains oriented with the  $\{10\bar{1}0\}$  planes perpendicular to the tensile or compression tests show only elastic behavior in the full stress range up to the sample fracture. As it was commented previously, in the alloy extruded at 623 K (350 °C), these are orientations for which both basal slips are more difficult.

#### IV. DISCUSSION

The increase of the extrusion temperature favors the complete recrystallization process in the magnesium  $\text{MgY}_2\text{Zn}_1$  alloy. However, compared to other magnesium alloys that exhibit a strong fiber texture with the basal plane parallel to the extrusion direction, the DRXed grains in  $\text{MgY}_2\text{Zn}_1$  alloy extruded at 723 K (450 °C) present a random texture. The recrystallization process in the Mg-Y-Zn alloys containing LPSO is controlled by a Particle Stimulated Nucleation process (PSN).<sup>[14]</sup> This process, typical in metal matrix composite, tends to develop a random texture in the matrix since grains nucleate around the particle where the stored plastic strain energy is higher.<sup>[29]</sup>

The randomization of magnesium grains tends to make the tension–compression asymmetry disappear in magnesium alloys because there are always grains appropriately oriented for the activation of the basal slip system.<sup>[30]</sup> In both cases, *in situ* diffraction experiments have demonstrated that the beginning of plasticity is always controlled by the activation of the basal slip system in random DRX grains. This can explain the low tension/compression ratio in both cases (near 0.9). Moreover, it is possible to estimate the increase in the yield stress of the alloy due to the refinement of the grains size given by the Hall–Petch relationship,  $\sigma_{\text{HP}} = k_{\text{HP}}D_{\text{DRX}}^{-1/2}$ . Using a slope value  $k_{\text{HP}} = 188 \text{ MPa } \mu\text{m}^{-1/2}$  calculated by Hagihara *et al.*<sup>[10]</sup> in a similar alloy, the increment of stress is 150 MPa, which is in good agreement with the experimental values (Figure 4). However, the activation of the basal slip does not explain the tension–compression asymmetry observed in both extrusion temperatures because it is independent of the stress sign.

It has been observed that the LPSO phase is highly deformed and oriented with the basal plane parallel to the extrusion direction for both extrusion temperatures. Plasticity in the 18R is controlled by the activation of the basal slip system with a CRSS of 10 MPa.<sup>[16]</sup> However, this slip system is inhibited under tension or compression along a direction parallel to the basal plane, which is the case of this study. Under this stress, non-basal slip or kinking at higher stresses has been reported.<sup>[16]</sup> This strong texture results in a tension–compression asymmetry in the LPSO phase. The yield stress is higher in compression than in tension. Garces *et al.*<sup>[19]</sup> have estimated an increment of around 11 MPa between

compression and tension with a 19 pct of volume fraction of LPSO which is slightly lower of the experimental values observed in Figure 4 (25 MPa). Therefore, the reinforcement contribution of the LPSO is underestimated. The evolution of the internal strains in the LPSO demonstrated that it bears an additional load transferred by the magnesium matrix especially from the alloy yield stress until the LPSO phase starts to deform plastically.

Although plasticity in  $\text{MgY}_2\text{Zn}_1$  alloy is initiated by the activation of the basal slip system, in compression the plastic deformation is controlled by the  $\langle 10\bar{1}1 \rangle \{10\bar{1}2\}$  tensile twinning, particularly in the alloy extruded at 623 K (350 °C). This is supported by the change in the crystallographic texture that intensifies the diffraction peak corresponding to the basal plane (see Figures 8 and 9). In the alloy extruded at 623 K (350 °C), twinning begins before the macroscopic yield stress in the non-DRXed grains. These grains are highly oriented with the basal plane parallel to the extrusion direction and yield at 300 MPa. In the alloy extruded at 723 K (450 °C), the beginning of the activation of tensile twinning occurs after the activation of basal slip system (200 MPa against 150 MPa, respectively). It is interesting to point out that twinning has been observed also in tension in the alloy extruded at 723 K (450 °C). DRXed magnesium grains are randomly oriented and, therefore, there are grains oriented with the basal plane perpendicular to the tensile axis which favors the activation of the  $\langle 10\bar{1}1 \rangle \{10\bar{1}2\}$  tensile twinning. The alloy extruded at 623 K (350 °C) does not show the activation of twinning under tension along the extrusion direction. Barnett *et al.*<sup>[24]</sup> have shown that the stress required for twinning increases with decreasing grain size more rapidly than stress required to activate slip. Therefore, the activation of deformation slip modes would be easier than twinning in DRXed grains in the alloy extruded at 623 K (350 °C) due to its fine grain size (0.9  $\mu\text{m}$ ).

#### V. CONCLUSION

The influence of the extrusion temperature on the tension–compression asymmetry has been studied in an  $\text{MgY}_2\text{Zn}_1$  alloy containing 19 pct of LPSO phase using neutron diffraction experiment during *in situ* tension and compression tests. The following conclusion can be drawn:

1. The texture of the alloy depends strongly on the extrusion temperature. At the lowest extrusion temperature, the recrystallization process is not completed and coarse areas of non-DRXed Mg grains, highly oriented with the basal plane parallel to the extrusion direction, are present. The DRXed Mg grains in the alloy are randomly oriented regardless of extrusion temperature. The LPSO phase, however, orients their basal plane parallel to the extrusion direction, at the two extrusion temperatures.
2. Independent of the stress sign and the extrusion temperature, the beginning of plasticity in the alloy is controlled by the activation of the basal slip system in the DRXed magnesium grains. The finer grain size in the alloy extruded at 623 K (350 °C) leads to a higher yield stress value.

3. Tensile twinning also takes place especially in compression, orienting the basal plane perpendicular to the compression axis. Tensile twinning occurs before macroscopic yield stress in the alloy extruded at 623 K (350 °C) and after macroscopic yield stress in the alloy extruded at 723 K (450 °C).
4. The tension–compression asymmetry presented in this alloy, where yield stress is higher in compression than in tension, is caused by the texture of the elongated LPSO phase. The basal plane is parallel to the extrusion direction which inhibits the activation of the basal slip system that is its main deformation system.

## ACKNOWLEDGMENTS

Authors would like to acknowledge the financial support from the Spanish Ministry of Economy and Competitiveness under project number MAT2016-78850-R and the Czech Science Foundation under the contract 16-12075S. We would like to acknowledge the expert support of Miguel Acedo and Edurne Laurin for assistance with the extrusion processing and the metallographical preparation, respectively. The neutron spallation source ISIS is acknowledged for the provision of beamtime at the ENGIN-X beamline. DESY (Hamburg, Germany) and FRM2 (Munich, Germany) are kindly acknowledged for beamtime on the beamlines P07 and STRESS-SPEC, respectively. We kindly acknowledge the support of the EU during the synchrotron and neutron measurements. The authors gratefully acknowledge the financial support provided by HZG and FRM II to perform the neutron scattering measurements at the Heinz Maier-Leibnitz Zentrum (MLZ), Garching, Germany.

## REFERENCES

1. A. Inoue, Y. Kawamura, M. Matsushita, K. Hayashi, and J. Koike: *J. Mater. Res.*, 2001, vol. 21, pp. 1894–1900.
2. M. Yamasaki, K. Hashimoto, K. Hagihara, and Y. Kawamura: *Acta Mater.*, 2011, vol. 59, pp. 3646–58.
3. G. Garcés, M. Maeso, I. Todd, P. Pérez, and P. Adeva: *J. Alloys Compd.*, 2007, vol. 432, pp. L10–14.
4. G. Garcés, E. Oñorbe, F. Dobes, P. Pérez, J.M. Antoranz, and P. Adeva: *Mater. Sci. Eng. A*, 2012, vol. 539, pp. 48–55.
5. Y. Jono, M. Yamasaki, and Y. Kawamura: *Mater. Trans.*, 2013, vol. 54, pp. 703–12.
6. E. Oñorbe, G. Garcés, F. Dobes, P. Pérez, and P. Adeva: *Mater. Trans. A*, 2013, vol. 44A, pp. 2869–83.
7. Y.M. Zhu, A.J. Morton, and J.F. Nie: *Acta Mater.*, 2010, vol. 58, pp. 2936–47.
8. D. Egusa and E. Abe: *Acta Mater.*, 2012, vol. 60, pp. 166–78.
9. M. Hirano, K. Yamasaki, K. Hagihara, and Y. Kawamura: *Mater. Trans.*, 2010, vol. 51, pp. 1640–47.
10. K. Hagihara, A. Kinoshita, Y. Sugino, M. Yamasaki, Y. Kawamura, H.Y. Yasuda, and Y. Umakoshi: *Acta Mater.*, 2010, vol. 58, pp. 6282–93.
11. G. Garces, M.A. Muñoz-Morris, D.G. Morris, P. Perez, and P. Adeva: *Mater. Sci. Eng. A*, 2014, vol. 614, pp. 96–105.
12. G. Garces, D.G. Morris, M.A. Muñoz-Morris, P. Perez, D. Tolnai, C. Mendis, A. Stark, H.K. Lim, S. Kim, N. Shell, and P. Adeva: *Acta Mater.*, 2015, vol. 94, pp. 78–86.
13. E. Oñorbe, G. Garcés, P. Pérez, S. Cabeza, M. Klaus, C. Genzel, E. Frutos, and P. Adeva: *Scr. Mater.*, 2011, vol. 65, pp. 719–22.
14. E. Oñorbe, G. Garcés, P. Pérez, and P. Adeva: *J. Mater. Sci.*, 2012, vol. 47, pp. 1085–93.
15. M. Tane, Y. Nagai, H. Kimizuka, K. Hagihara, and Y. Kawamura: *Acta Mater.*, 2013, vol. 61, pp. 6338–51.
16. K. Hagihara, N. Yokotani, and Y. Umakoshi: *Intermetallics*, 2010, vol. 18, pp. 267–76.
17. G. Garces, M.A. Munoz-Morris, D.G. Morris, J.A. Jimenez, P. Perez, and P. Adeva: *Intermetallics*, 2014, vol. 55, pp. 167–76.
18. S. Kleiner and P.J. Uggowitzer: *Mater. Sci. Eng. A*, 2004, vol. 379, pp. 258–63.
19. G. Garces, P. Perez, S. Cabeza, H.K. Lin, S. Kim, W. Gan, and P. Adeva: *Mater. Sci. Eng. A*, 2015, vol. 647, pp. 287–93.
20. C. Randau, H.G. Brokmeier, W.M. Gan, M. Hofmann, M. Voeller, W. Tekouo, N. Al-hamdany, G. Seidl, and A. Schreyer: *Nucl. Instr. Meth. Phys. Res. A*, 2015, vol. 794, pp. 67–75.
21. J.R. Santisteban, M.R. Daymond, L. Edwards, and J.A. James: *J. Appl. Cryst.*, 2006, vol. 39, pp. 812–25.
22. G. Garces, G. Requena, D. Tolnai, P. Perez, P. Adeva, A. Stark, and N. Schell: *J. Mater. Sci.*, 2014, vol. 49, pp. 2714–22.
23. G. Garcés, G. Requena, D. Tolnai, P. Pérez, P. Adeva, J.A. Jiménez, A. Stark, and N. Schell: *Rev. Metal.*, 2015, vol. 51, p. e043, DOI:10.3989/revmetalm.043.
24. M.R. Barnett, Z. Keshavarz, A.G. Beer, and D. Atwell: *Acta Mater.*, 2004, vol. 52, pp. 5093–5103.
25. S.R. Agnew, D.W. Brown, and C.N. Tome: *Acta Mater.*, 2006, vol. 54, pp. 4841–52.
26. E.A. Brandes and G.B. Brooks (eds.): *Smithells Metals Reference Book*, 15-2. Butterworth-Heinemann, London.
27. M.A. Gharghour, G.C. Weatherly, J.D. Embury, and J. Root: *Philos. Mag. A*, 1999, vol. 79, pp. 1671–95.
28. B. Clausen, C.N. Tomé, D.W. Brown, and S.R. Agnew: *Acta Mater.*, 2008, vol. 56, pp. 2456–68.
29. G. Garcés, P. Pérez, and P. Adeva: *Scr. Mater.*, 2005, vol. 52, pp. 615–19.
30. E.A. Ball and P.B. Prangnell: *Scr. Met. Mater.*, 1994, vol. 31, pp. 111–16.